

# Digital camera workflow for high dynamic range images using a model of retinal processing

Daniel Tamburrino<sup>a</sup>, David Alleysson<sup>b</sup>, Laurence Meylan<sup>a</sup>, and Sabine Süsstrunk<sup>a</sup>

<sup>a</sup>School of Computer and Communication Sciences, Ecole Polytechnique Fédérale de Lausanne (EPFL), Switzerland

<sup>b</sup>Psychology and NeuroCognition Laboratory, CNRS UMR 5105, Université Pierre-Mendes France (UPMF), Grenoble, France

## ABSTRACT

We propose a complete digital camera workflow to capture and render high dynamic range (HDR) static scenes, from RAW sensor data to an output-referred encoded image. In traditional digital camera processing, demosaicing is one of the first operations done after scene analysis. It is followed by rendering operations, such as color correction and tone mapping. In our workflow, which is based on a model of retinal processing, most of the rendering steps are performed before demosaicing. This reduces the complexity of the computation, as only one third of the pixels are processed. This is especially important as our tone mapping operator applies local and global tone corrections, which is usually needed to well render high dynamic scenes. Our algorithms efficiently process HDR images with different keys and different content.

**Keywords:** high dynamic range, tone mapping, retinal processing, digital camera workflow, sharpening, halo artifacts

## 1. INTRODUCTION

High dynamic range\* (HDR) imaging is becoming more and more popular. Most of today's digital cameras, however, are not yet HDR-capable. To create HDR image files, several shots of the same scene at different exposures have to be taken, and dedicated software has to be used to create an HDR image. It is foreseeable that digital cameras will soon incorporate the functionality to automatically generate HDR images in the camera itself. Sensor manufacturers also continue to increase the dynamic range that can be captured with their sensors.

Although HDR displays are being developed, such as by Dolby,<sup>1</sup> they are not yet generally available. A need thus exists to compress the dynamic range of the HDR image to the standard dynamic range (SDR) of displays or prints. Tone mapping algorithms perform this adaptation of dynamic range. The aim of tone mapping is usually to produce pleasing images that match the perception of the original scene.

Figure 1 illustrates some tone mapping algorithms. Global algorithms, such as gamma correction (Fig. 1(a)) are commonly used on SDR images, but perform poorly on HDR images. They tend to compress the tonal range too much, reducing edge contrast and thus visibility of details. Local methods, as illustrated in Fig. 1(b), allow maintaining good local contrast in all parts of the image. The drawback of these local tone mappers is that they are often not computationally efficient, as they do adaptive filtering operations.

In traditional digital camera workflows, demosaicing is one of the first operations performed after scene analysis.<sup>2</sup> It is followed by rendering operations, such as color correction and tone mapping. In our approach, which is based on a model of retinal processing of the human visual system (HVS), rendering operations including adaptation are performed directly on the CFA image. Our workflow thus conforms more closely to the retinal processing model, where adaptation is performed on the cone mosaic before demosaicing. Thus, the computation cost is reduced by three, as only one third of the values are present in the mosaic image.

We apply our workflow on different kinds of scenes with varying dynamic range and key. The images are visually pleasing and do not show visible artifacts (see Fig. 1(c) and Fig. 1(d), and Section 4).

---

Further author information:

E-mail: daniel.tamburrino@epfl.ch

\*Dynamic range is defined as the luminance ratio of the brightest and darkest object in the scene.



(a)



(b)



(c)



(d)

Figure 1. Different rendering methods for HDR images. (a) Gamma correction with  $\gamma = 2.4$ . (b) Photoshop<sup>3</sup> local adaptation method. (c) and (d) Our proposed method.

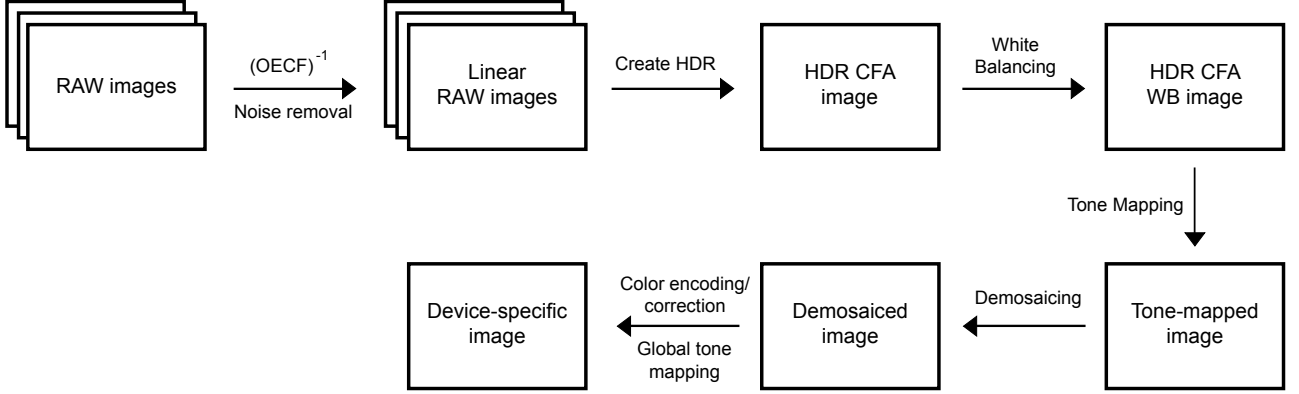


Figure 2. Complete workflow from RAW sensor data to output device-dependent image.

The different steps of our workflow, as illustrated in Fig. 2, are developed in the following section. First, several linear RAW images are combined to create an HDR image. We then perform white balancing. After that, tone mapping is applied to compress the dynamic range of the HDR image to the dynamic range of a standard device. Next, demosaicing reconstructs the missing color values. Finally, color and global tone correction improve image appearance on the output device. The influence of the tone mapping algorithm parameters on local contrast enhancement, sharpening, and artifacts is discussed in Section 3. Finally, images rendered with our workflow are presented in Section 4.

## 2. WORKFLOW

We are using data from a Canon 350D digital camera (also called Digital Rebel XT) that produces 12-bit RAW sensor data. The RAW data is extracted from the Canon *.CR2* file using the freeware tool *dcraw*.<sup>4</sup> The optoelectronic conversion function (OECF) of the RAW data is measured using an OECF test chart uniformly lit by an integration sphere, using the method presented in ISO 14524.<sup>5</sup> The RAW data of our Canon camera is almost linear. The inverse OECF is computed and applied to the RAW sensor data to obtain perfectly linear values.

### 2.1 Creating HDR images

The initial two steps in the proposed digital camera workflow do not differ significantly from usual camera processing. We first produce a CFA RAW HDR image, i.e. a single layer color filter array image with an extended dynamic range. When the dynamic range of the scene is higher than the dynamic range of the sensor, a multi-exposure technique can be applied to capture the whole dynamic range of the original scene. Multiple shots of the same scene are taken with different exposure times. This limits our application to static scenes, but with different camera technology (HDR cameras), the proposed workflow can also work on dynamic HDR scenes.

After linearizing the images using the inverse OECF and removing the dark current, the RAW images are combined to create a CFA HDR image using a method based on the algorithm by Debevec and Malik.<sup>6</sup> Our method is simpler as the input images are linear and thus there is no need to estimate the non-linearity inherent to processed images. We therefore combine the pixels from the images with different exposure times as follows:

$$P_{HDR} = \frac{1}{|V|} \sum_{P_i \in V} \frac{t_{ref}}{t_i} P_i, \quad (1)$$

where  $V$  is a subset of non saturated pixel values,  $t_{ref}$  is the reference exposure time to which the pixel values are compensated,  $t_i$  is the exposure time corresponding to pixel value  $P_i$ , and  $P_{HDR}$  is the new pixel value.

## 2.2 White balancing

The second step of our workflow is to perform white balancing of the CFA RAW HDR image. White balancing is done by weighting each RGB channel, i.e. the sub-mosaics that contain either the existing red, green, and blue filter responses, with a coefficient that depends on the illuminant and the quantum efficiencies of the sensor and color filters. The corrected pixel values are obtained as follows:

$$\begin{bmatrix} R_{WB} \\ G_{WB} \\ B_{WB} \end{bmatrix} = \begin{bmatrix} a & 0 & 0 \\ 0 & b & 0 \\ 0 & 0 & c \end{bmatrix} \begin{bmatrix} R_C \\ G_C \\ B_C \end{bmatrix}, \quad (2)$$

where  $b$  is usually set to 1 and  $a$  and  $c$  are adapted consequently. The subscript  $WB$  stands for *white balanced* and  $C$  for *camera*. The values for  $a$  and  $c$  are calculated based on the measured quantum efficiencies of the sensor and color filter combinations and the camera responses of the illuminant.

## 2.3 Tone mapping

We then apply tone mapping directly on the CFA image. The goal of tone mapping in digital photography usually is to render images that match our perception by adapting the scene's dynamic range to the output device's dynamic range. Tone mapping is particularly important for compression of HDR images. Tone mapping algorithms can either be global or local. Global methods,<sup>7,8</sup> which can use gamma, logarithmic, or sigmoidal functions, are not suited for HDR image compression to standard dynamic range (SDR) for use on devices such as current computer displays or prints. Indeed, global algorithms tend to compress the tonal range too much, causing a loss of detail visibility (Fig. 1(a)). The human visual system (HVS), on the other hand, is able to process the data and to adapt to a large dynamic range by locally processing the image, allowing details to be visible in the shadows as well as in the highlights. Thus, local *and* global algorithms perform better on HDR images than global algorithms alone.

A number of local tone mapping algorithms are described in the literature.<sup>9-11</sup> Our tone mapping algorithm is inspired by the non-linear processing that takes place in the retina on the cone mosaic,<sup>12</sup> as illustrated in Fig. 3. We model the processes that take place in both the outer plexiform layer (OPL) and inner plexiform layer (IPL) of the retina. The bipolar and ganglion cells only transmit the information from one layer to the next, whereas the horizontal and amacrine cells play a role in the non-linear processing. The horizontal cells take the L, M, and S cone responses as input, which we equate to the mosaic CFA image. The horizontal cells process the input signal taking into account the surrounding cones, i.e. pixels in the digital case. The output is passed to the bipolar cells. The amacrine cells then perform the same kind of operations as the horizontal cells. Finally, the output is passed to the ganglion cells.

The two non-linear processes are modeled using the Naka-Rushton<sup>13</sup> function in the following form:

$$Y = \alpha \frac{X}{X + X_0}, \quad (3)$$

where  $X$  is the input light intensity,  $X_0$  is an adaptation factor,  $Y$  is the adapted signal, and  $\alpha$  is a normalization factor.

In our tone mapping algorithm, equation 3 is as follows. To model the OPL processing:

$$I_{bip}(p) = (I_{CFA}(max) + H(p)) \frac{I_{CFA}(p)}{I_{CFA}(p) + H(p)}, \quad (4)$$

where  $p$  is a pixel in the image,  $I_{CFA}$  is the normalized digital count of the input mosaic image,  $H(p)$  is the adaptation factor of the horizontal cells, and  $I_{bip}$  the normalized output of the bipolar cells.

The output of the previous equation  $I_{bip}$  is similarly processed and models the processing of the IPL layer:

$$I_{ga}(p) = (I_{bip}(max) + A(p)) \frac{I_{bip}(p)}{I_{bip}(p) + A(p)}, \quad (5)$$

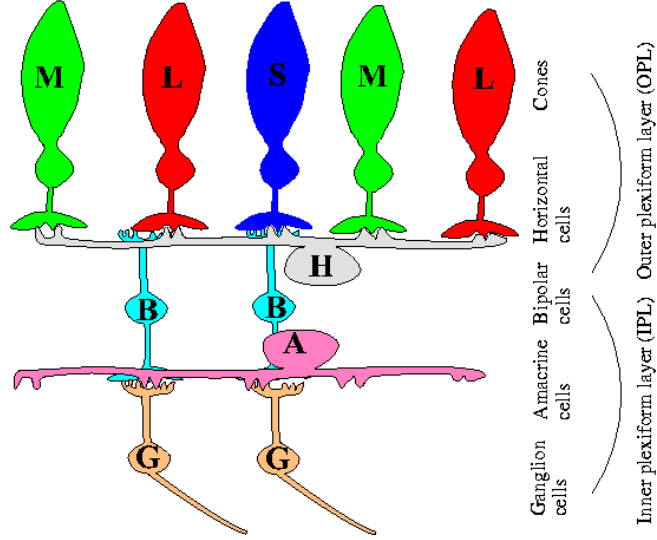


Figure 3. Simplified model of the retina.

where  $A(p)$  is the adaptation factor of the amacrine cells and  $I_{ga}$  is the output of the ganglion cells.

The main difference with the original Naka-Rushton equation is that in our approach, the adaptation factor is pixel dependent. This factor is a weighted average of surrounding pixel values plus a global factor that depends on the key of the image:

$$H(p) = (I_{CFA} * G_H)(p) + \kappa \overline{I_{CFA}} \quad (6)$$

and

$$A(p) = (I_{bip} * G_A)(p) + \kappa \overline{I_{bip}}, \quad (7)$$

where  $\kappa$  is a coefficient that depends on the key of the image,  $*$  denotes the convolution operation, and  $\overline{I_{CFA}}$  and  $\overline{I_{bip}}$  correspond to the mean value of  $I_{CFA}$  and  $I_{bip}$ , respectively. The filters  $G_H$  and  $G_A$  are two-dimensional Gaussian filters with spatial constant  $\sigma_H$  and  $\sigma_A$ , respectively:

$$G_{H,A}(x, y) = e^{-\frac{x^2+y^2}{2\sigma_{H,A}^2}}, \quad (8)$$

where  $x$  and  $y$  are pixel locations.

The parameters to optimize rendering for all types of image keys and content are  $\kappa$  and  $\sigma$ . In Section 3, we discuss the influence of these parameters on local contrast enhancement, sharpening, and quality of the results.

## 2.4 Demosaicing

Next, the tone mapped images are demosaiced. The goal is to estimate the missing pixel values from the CFA image. Although any demosaicing algorithm can be used, we apply the linear demosaicing described by Alleysson et al.<sup>14</sup> As the previous two non-linear processing blocks in the workflow tend to enhance the contours of the image and amplify the noise, we use a slightly different luminance estimation filter than in Alleysson et al. This new filter removes more high frequencies and thus reduces noise:

$$F_{dem} = \frac{1}{256} \begin{bmatrix} 1 & 4 & 6 & 4 & 1 \\ 4 & 16 & 24 & 16 & 4 \\ 6 & 24 & 36 & 24 & 6 \\ 4 & 16 & 24 & 16 & 4 \\ 1 & 4 & 6 & 4 & 1 \end{bmatrix}. \quad (9)$$

## 2.5 Post-Processing

Finally, the demosaiced image is corrected and transformed to an output-referred color image encoding. This processing includes color correction and global tone mapping.

### 2.5.1 Color Correction

Color correction transforms the camera-specific RGB values to a standard color encoding. Color correction is performed with a linear transformation of the white-balanced camera RGB values to the desired color space values. An example of such a color space is sRGB:

$$\begin{bmatrix} R_{sRGB} \\ G_{sRGB} \\ B_{sRGB} \end{bmatrix} = M_{3 \times 3} \begin{bmatrix} R_{WB} \\ G_{WB} \\ B_{WB} \end{bmatrix} \quad (10)$$

The transformation matrix  $M$  is a concatenation of the  $3 \times 3$  matrix that converts white-balanced camera RGB values to tristimulus values, the  $3 \times 3$  diagonal matrix that adapts for the desired white-point, and the  $3 \times 3$  matrix that is specified in the conversion from XYZ to standard color space, as for example for sRGB.<sup>15</sup>

It is not trivial to compute the camera RGB to XYZ transform, as camera spectral sensitivities almost never follow the Luther condition.<sup>16</sup> We compute the matrix with a white-point preserving least-square (WPPLS) method<sup>17</sup> using either the camera sensor spectral responses (called *maximum ignorance data set*) or a set of known XYZ values from a color chart.

Color correction is performed after demosaicing as it requires the three RGB values at each pixel location, whereas in a CFA image only one color information per pixel location is present.

### 2.5.2 Global Tone Mapping

The tone mapping algorithm described in Section 2.3 already performs global tone correction that can be modulated with the  $\kappa$  factor. As will be discussed in Section 3.3, varying  $\kappa$  is equivalent to applying a gamma power function on the output image. Therefore, a simple image-dependent gamma correction coupled with a luminance histogram stretching is performed to obtain the final output image.

## 3. EFFECT OF TONE MAPPING PARAMETERS

The goal of tone mapping may vary depending on the application and intent. Tone mapping can, for example, be used to produce an image with as many details as possible, even though this rendering might look unrealistic. The aim is generally to produce a pleasant image on an output device that matches the perception of the original scene. For an HDR image, this implies increasing local contrast to reveal details in the shadows and highlights while keeping the overall image look “natural”.

In this section, the different parameters involved in our tone mapping algorithm and their effect on local contrast, sharpening, and artifacts are discussed in more details on a toy example: a simple 1D step-like signal that represents an edge  $\Psi(x)$  from a piece-wise constant region  $\Psi(x) = a$  to a piece-wise constant region  $\Psi(x) = b$ , where  $x$  is the pixel location and  $\Psi(x)$  is the pixel value (Fig. 4(a)). Considering this basic input signal  $\Psi(x)$ , the shape of the output signal  $\Phi(x)$  (Fig. 4(b)) will depend on several parameters, among which  $\sigma_{H,A}$ , the global factor  $\kappa$ , the start digital value of the signal, the start and end digital value of the edge, its amplitude, and its relative sharpness.

### 3.1 Filter Sizes: Local Contrast, Sharpening, and Artifacts

In the proposed tone mapping algorithm, the non-linearity based on the Naka-Rushton equation is applied twice, with two gaussian filters of spatial constant  $\sigma_H$  and  $\sigma_A$ , respectively. The implied difference of Gaussian (DOG) filtering results in a sharpening effect,<sup>18</sup> which also increases the local contrast. Under certain conditions, these non-linear operators also introduces halo artifacts that appear as a dark border along edges.

Applying only the first non-linearity with  $\sigma_H$  to the input signal  $\Psi(x)$  produces the signal  $\Phi(x)$  as an output (Fig. 4(b)), which exhibit a well that can be characterized by an amplitude  $\delta$  and a width  $\omega$ . The amplitude  $\delta$

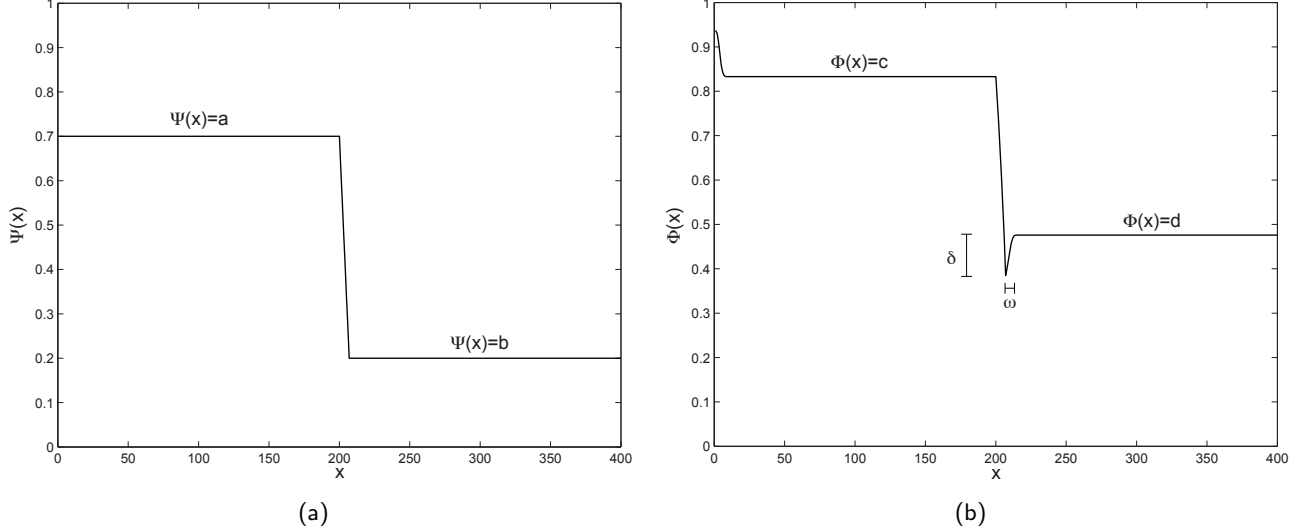


Figure 4. Effect of the tone mapping operator on a simple 1D signal. (a) Signal  $\Psi(x)$  representing an edge. (b) Signal  $\Phi(x)$  after applying the first non-linearity of the tone mapping operator on  $\Psi(x)$  with  $\sigma_H = 1.5$  and  $\kappa = 1$ .

is defined as the difference between the right part of the output signal  $\Phi(x) = d$  and the minimum value of the edge, i.e. the amplitude of the well. The width  $\omega$  is defined as the maximum width of the well.

The well's amplitude  $\delta$  represents an increase in local contrast and sharpening. Under certain conditions, discussed later in this section, this well can also introduce halo artifacts, as the digital value at the edge  $\Phi(\text{edge})$  is darkened and it might visually look like a dark border along edges. Figure 5 illustrates the variation of  $\omega$  and  $\delta$  relatively to  $\sigma_H$ , that represents the spatial constant of a gaussian filter. On one hand, the width  $\omega$  of the well is increasing linearly with the size of  $\sigma_H$  (Fig. 5(a)), which is consistent with the averaging function of the gaussian filter. On the other hand, the amplitude  $\delta$  is increasing as a log-like function, with a maximum value obtained for a relatively low  $\sigma_H$  value (Fig. 5(b)). For bigger  $\sigma_H$  values, the width  $\omega$  is still increasing, whereas the amplitude  $\delta$  remains constant. As local contrast and sharpening are principally induced by the amplitude  $\delta$ , there is no need to use large  $\sigma_H$  values. The use of small gaussian filters obviously also improves computational efficiency.

The second stage of the tone mapping algorithm with parameter  $\sigma_A$  doesn't change the general shape of the output signal (Fig. 6(a)), but it amplifies the amplitude and width of the well. The width increases linearly, whereas the amplitude increases in a log-like manner. However, the effect on the amplitude  $\delta$  is relatively smaller (Fig. 6(b)) than in the first stage with  $\sigma_H$  (Fig. 5(b)).

Other parameters, including  $\kappa$ , signal and edge properties, influence the amplitude  $\delta$  but not the width  $\omega$ . However, these parameters are strongly correlated with the signal and cannot be arbitrarily chosen. They must be considered as fixed by the image content and properties, and the  $\sigma_{H,A}$  values adapted accordingly.

### 3.2 Sharpening vs. Halo Artifacts

The way the tone mapping algorithm works almost always introduces a well at edges, which increases the sharpness with the amplitude  $\delta$ . Under certain conditions, this well becomes visible as a halo artifact along edges in the image. This artifact gets more important with the increase of  $\sigma_{H,A}$ , as the amplitude and width of the well increase. There is thus a trade-off between local contrast enhancement, sharpening, and artifacts. However, the visibility of the halos not only depends on the tone mapping parameters, but also on the type of image, the kind of edges it contains (sharp or smooth, high or low contrast), and more importantly on the output device and viewing conditions. The halo will become visible only if the HSV is able to detect it.

For a given image, the amount of sharpening that has to be applied will also depend on the output device, its size, its resolution, and the viewing conditions. Consider as a typical application a scene acquired with a high

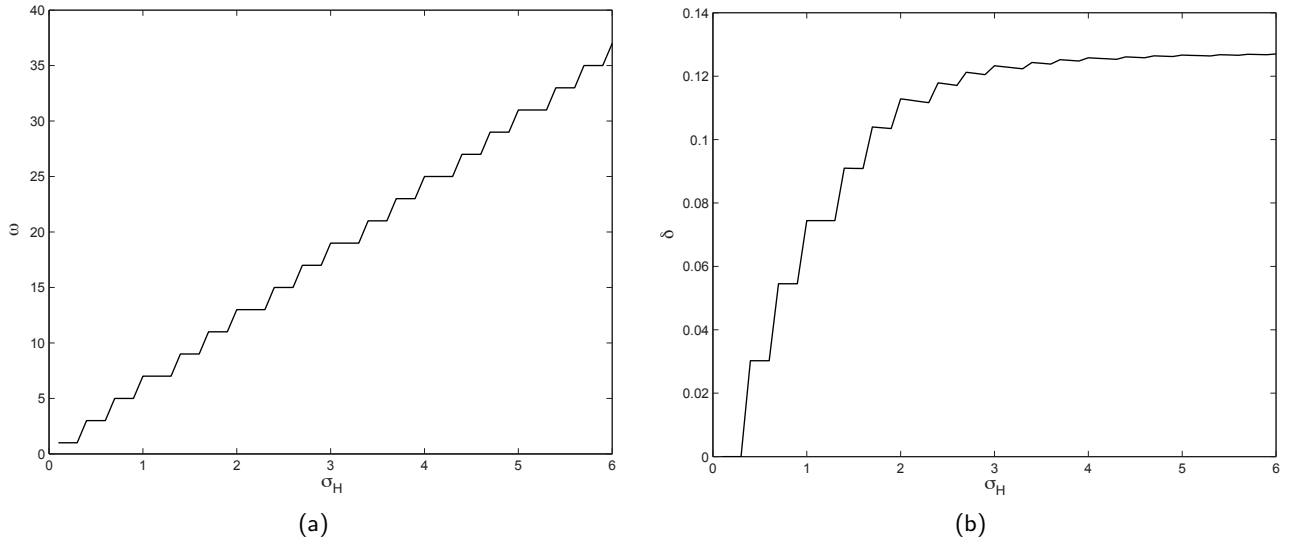


Figure 5. Effect of the gaussian filter size with spatial constant  $\sigma_H$  on the well (Fig. 4(b)) of width  $\omega$  and amplitude  $\delta$ . (a) The width  $\omega$  varies linearly with the increase of  $\sigma_H$ . (b) The amplitude  $\delta$  increases in a log-like manner with the increase of  $\sigma_H$ .

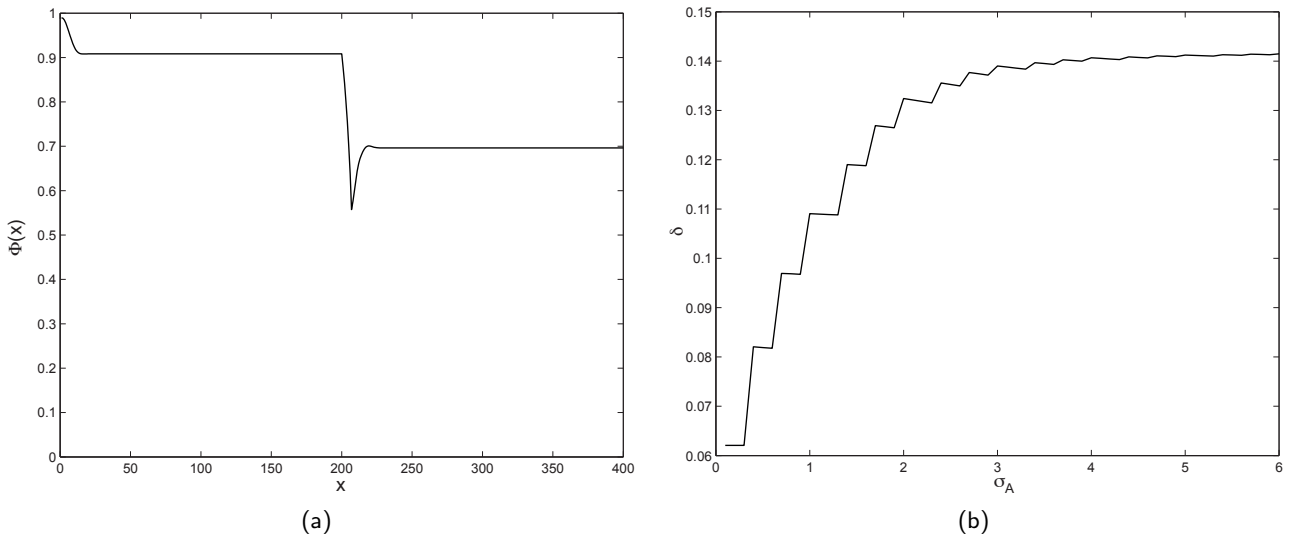


Figure 6. (a) Output of the second non-linearity applied to the signal of Fig. 4(b) with a  $\sigma_H = 1.5$  and  $\sigma_A = 3$ . (b) The amplitude  $\delta$  increases in a log-like manner with the increase of  $\sigma_A$ .



resolution digital camera and rendered through our workflow in order to print a small 10x15 cm photo viewed at a distance of 30 cm. Such prints generally have a large amount of sharpening applied to produce pleasant images. More sharpening implies a bigger  $\delta$  and  $\omega$ . Both factors influence the halo:  $\delta$  for how dark is the edge surround, and  $\omega$  for the halo width. However, considering the high resolution of the acquired image and small size of the print, a lot of sharpening can be applied before seeing any artifact. Of course, taking the same rendered image and viewing distance, but printing it to an A3 paper size, may lead to visible halo artifacts.

The size of  $\sigma_{H,A}$  must be computed for each specific application to avoid halo artifacts. The halo width will generally depend on the output device resolution and viewing distance. The halo intensity will depend on the dynamic range of the output device and also strongly on the dynamic range of the captured scene and its highest contrast edge. As we discussed earlier, the amount of sharpening is limited to relatively small  $\sigma_{H,A}$  values. The width of the halo is therefore also limited as there is no need to go beyond those  $\sigma_{H,A}$  values: it would only increase the halo, not sharpening. The first filter coefficient  $\sigma_H$  can also generally be chosen smaller than the second one,  $\sigma_A$ , as  $\sigma_H$  has more effect on the well's amplitude and thus on visibility of halos.

### 3.3 Global Parameter and Post Processing

The  $\kappa$  parameter weights the global variable of the adaptation factor in the non-linear tone mapping equations (Eq. 4 to 7). Although  $\kappa$  can be chosen independently for the ganglion and the amacrine adaptation factors, our experiments showed that similar results can be achieved by choosing a unique value for  $\kappa$  in both stages of the processing.

The global parameter has several effect on the output image. It tends to darken the image and compress the shadows. At edges, the amplitude  $\delta$  diminishes as  $\kappa$  increases, but the overall difference  $\Phi(c) - \Phi(d)$  remains more or less constant. However, the global factor cannot be tuned to reduce halo artifacts. In fact, this  $\kappa$  factor acts like a global tone mapping operator and its value is image dependent. The amount of global correction is related to the key of the image. High and low key are terms used to describe images that have a higher-than-average and lower-than-average mean intensity, respectively.<sup>12</sup> A low key image will need a bigger  $\kappa$  value to compensate for the local contrast enhancement, which tends to grey-out parts of the image that should look black. The key-dependency, however, is not trivial. Indeed, the way the key is computed is primordial. Considering two scenes with the same content, but one with a specular highlight and the other without, the average luminance will be different, although the  $\kappa$  parameter should remain the same to produce the same pleasant image.

As no robust relation between the key and  $\kappa$  was yet found, we decided to set  $\kappa = 1$ , a value which gives good results for average images. The global correction is done in the post-processing step of the workflow in the form of a gamma correction. Experiments showed that there is a strong correlation between the  $\kappa$  value and the gamma value that produce similar looking results. This allows to easily and quickly fine-tune the output image according to its content or user's preference.

## 4. RESULTS

The tone mapping algorithm was tested on a wide range of HDR images, available online.<sup>19–21</sup> The entire workflow, however, could only be tested on our own set of images, as unprocessed RAW files and camera characterization data are generally not available online. Some of the workflow parameters are highly correlated to the camera and must be computed for each camera make and model. In this section, we present results of our workflow applied on several images. The results are shown and the different parameters are discussed. All the RAW data, the figures, and the code used to produce them are available online.<sup>21</sup>

Some images produced by our workflow are presented in Fig. 7. These images are compared to Adobe Photoshop CS3's<sup>3</sup> rendering workflow, which is the only known software that performs a full HDR workflow from input RAW files to an output referred encoded image. The RAW data files are opened with Photoshop's *Merge to HDR* function to produce an HDR file. The resulting HDR image is then converted to SDR using Photoshop's local tone adaptation with default parameters.

The sharpening effect is illustrated in Fig. 8 where Fig. 8(b) uses bigger  $\sigma_{H,A}$  values than Fig. 8(a), thus producing more sharpening. Increasing the size of the  $\sigma_{H,A}$  (Fig. 8(c)) values introduces halo artifacts along



(a)



(b)



(c)



(d)



(e)



(f)



(g)



(h)

Figure 7. (a, c, e, g) Images produced by our workflow with  $\sigma_H = 1.5$  and  $\sigma_A = 3$ . (b, d, f, h) Images produced with Photoshop.<sup>3</sup>



Figure 8. Illustration of sharpening and halo artifacts. (a) Image rendered with  $\sigma_H = 0.5$  and  $\sigma_A = 1.5$ . (b) Image rendered with  $\sigma_H = 1.5$  and  $\sigma_A = 3$ . The edges are sharper than in (a). (c) Image rendered with  $\sigma_H = 3$  and  $\sigma_A = 4$ . The sharpening effect is too strong and visually looks like halo artifacts along high contrast edges.

high contrast edges. Artifacts along edges are more visible when looking at this magnified part of the image, as the viewing conditions changed as discussed in Section 3.2.

In general, parameters that produce pleasing images with no visible artifacts can be chosen for any specific application under any viewing conditions.

## 5. CONCLUSION AND FUTURE WORK

We developed a new digital camera workflow for HDR images inspired by HVS retinal processing. Most of the rendering operations are applied before demosaicing. The proposed tone mapping algorithm performs local and global corrections. As most operations are performed on a single layer image and as the spatial filtering in the tone mapping operator uses small filters, the computational complexity of the workflow is reduced compared to concurrent approaches.

This new workflow provides satisfactory results on most images. The amount of sharpening and artifacts can be controlled based on the rendering intent and output device. In the future, we will investigate how to perform all rendering steps before demosaicing, including color correction.

## ACKNOWLEDGMENTS

The work presented in this paper was in part supported by the Swiss National Science Foundation under grant number 200021-113829.

## REFERENCES

1. <http://www.dolby.com/promo/hdr/technology.html>.
2. J. Holm, I. Tastl, L. Hanlon, and P. Hubel, *Colour Engineering: Achieving Device Independent Colour*, ch. 9, Color processing for digital photography, pp. 179–220. John Wiley and Sons, 2002.
3. <http://www.adobe.com/products/photoshop/>.
4. <http://www.cybercom.net/~dcoffin/dcraw/>.
5. ISO-14524, *Photography - Electronic Still Picture Cameras - Methods for measuring opto-electronic conversion functions (OECFs)*, 1999.
6. P. E. Debevec and J. Malik, “Recovering high dynamic range radiance maps from photographs,” in *Proceeding of SIGGRAPH*, 1997.

7. K. Devlin, "A review of tone reproduction techniques," Tech. Rep. CSTR-02-005, Department of Computer Science, University of Bristol, 2002.
8. G. J. Braun and M. D. Fairchild, "Image lightness rescaling using sigmoidal contrast enhancement functions," *Journal of Electronic Imaging* **8**(4), pp. 380–393, 1999.
9. L. Meylan and S. Ssstrunk, "High dynamic range image rendering with a retinex-based adaptive filter," *IEEE Transactions on Image Processing* **15**(9), pp. 2820–2830, 2006.
10. E. Land and J. McCann, "Lightness and retinex theory," *Journal of The Optical Society of America* **61**(1), pp. 1–11, 1971.
11. F. Durand and J. Dorsey, "Fast bilateral filtering for the display of high-dynamic-range images," in *Proceedings of ACM SIGGRAPH 2002, Annual Conference on Computer Graphics*, pp. 257–266, 2002.
12. L. Meylan, D. Alleysson, and S. Ssstrunk, "A model of retinal local adaptation for the tone mapping of color filter array images," *Journal of Optical Society of America A* **24**(9), pp. 2807–2816, 2007.
13. K.-I. Naka and W. A. Rushton, "S-potentials from luminosity units in the retina of fish (cyprinidae)," *J. Physiology* **185**(3), pp. 587–599, 1966.
14. D. Alleysson, S. Ssstrunk, and J. Hrault, "Linear demosaicing inspired by the human visual system," *IEEE Transactions on Image Processing* **14**(4), pp. 439–449, 2005.
15. IEC:61966-2-1, *Multimedia systems and equipment - Colour measurement and management - Part2-1: Colour management - Default RGB colour space - sRGB*, 1999.
16. J. Nakamura, ed., *Image Sensors and Signal Processing for Digital Still Cameras*, CRC Press, 2006.
17. G. D. Finlayson and M. S. Drew, "Constrained least-squares regression in color spaces," *Journal of Electronic Imaging* **6**(4), pp. 484–493, 1997.
18. W. K. Pratt, *Digital Image Processing*, Wiley, 1991.
19. [http://www.cis.rit.edu/mcsl/icam/hdr/rit\\_hdr/](http://www.cis.rit.edu/mcsl/icam/hdr/rit_hdr/).
20. <http://www.cis.rit.edu/fairchild/HDRPS/HDRthumbs.html>.
21. [http://ivrg.epfl.ch/supplementary\\_material/index.html](http://ivrg.epfl.ch/supplementary_material/index.html).